SUPPORTING INFORMATION

Water-induced fluorescence enhancement of lead-free cesium bismuth halide quantum dots by 130% for stable white light-emitting devices

Zhuang-Zhuang Ma,[a] Zhi-Feng Shi,*[a] Lin-Tao Wang,[a] Fei Zhang,[a] Di Wu,[a] Dong-Wen Yang,*[a] Xu Chen,[a] Yu Zhang,[b] Chong-Xin Shan[a] and Xin-Jian Li[a]

[a]Key Laboratory of Materials Physics of Ministry of Education, School of Physics and Microelectronics, Zhengzhou University, Daxue Road 75, Zhengzhou 450052, China

[b]State Key Laboratory on Integrated Optoelectronics, College of Electronic Science and Engineering, Jilin University, Qianjin Street 2699, Changchun 130012, China

*Author to whom correspondence should be addressed. Electronic mail: shizf@zzu.edu.cn; yangdw@zzu.edu.cn

EXPERIMENTAL SECTION

Materials. CsCl (≥99.9%), CsBr (≥99.9%), $PbCl_2$ (≥99.9%), $PbBr_2$ (≥99.9%), and CsI (≥99.9%) were purchased from Xi'an Polymer Light Technology Corp. $BiCl_3$ (99%), $BiBr_3$ (99%), and BiI_3 (99%) were purchased from Alfa Aesar. Oleic acid (OA, 90%), n-octylamine (OLAM, 99%), and oleylamine (OAm, 90%) were purchased from Sigma-Aldrich. N,N-dimethylformamide (DMF), ethanol anhydrous, toluene, and DMSO were purchased from Beijing Chemical Reagent Co., Ltd., China. All the chemicals were used without further purification.

Synthesis of $Cs_3Bi_2X_9$ QDs. Typically, colloidal $Cs_3Bi_2Br_9$ QDs were fabricated by the ligand-assisted recrystallization method, which is described in the following section. In a typical synthesis of $Cs_3Bi_2Br_9$ QDs, 0.36 mmol CsBr and 0.24 mmol $BiBr_3$ were dissolved in 3 mL of DMSO, then 30 μL of OLAM and 0.6 mL of OA were added into the mixture solution to form a clear precursor solution at RT. Then, 0.5 mL of the precursor solution was injected into a toluene solution (5 mL) under vigorous stirring. After a reaction for 15 min, a crude solution emitting strong blue under UV light irradiation was obtained. Then the crude solution was centrifuged at 10000 rpm for 10 min to discard the large particles. After that, a bright blue colloidal $Cs_3Bi_2Br_9$ QDs solution was obtained for characterization and anion exchange. The solid powders of $Cs_3Bi_2Br_9$ QDs were obtained by gradient centrifugation of the crude solution at 5000 rpm and then 10000 rpm both for 10 min. $Cs_3Bi_2Cl_9$ QDs and $Cs_3Bi_2I_9$ QDs were fabricated by varying the precursors and solvents following a similar method. For adjusting the emission wavelength of the $Cs_3Bi_2X_9$ QDs, an anion-exchange technology was employed, in which CsCl or CsI dissolved in DMSO was quickly added into the as-prepared colloidal $Cs_3Bi_2Br_9$ QDs solution.

Water Treatment of $Cs_3Bi_2Br_9$ QDs. 1 mL deionized water was introduced into a 4 mL cuvette containing 2 mL of $Cs_3Bi_2Br_9$ QDs toluene solution. The cuvette was placed at room temperature for 0.5 h as an optimum treatment time and then the supernatant $Cs_3Bi_2Br_9$ QDs toluene solution

was separated from the water. Further, the supernatant is centrifuged and redispersed in toluene to obtain stable and high PLQY $Cs_3Bi_2Br_9$/BiOBr nanocomposites.

Synthesis of $CsPbBr_3$ and $CsPbCl_{1.5}Br_{1.5}$ QDs. 0.2 mmol $PbBr_2$, 0.2 mmol CsBr, 0.5 mL OA, and 0.25 mL OAm were added into the DMF (5 mL) to form a precursor solution. 0.5 mL of the precursor solution was injected into 5 mL of toluene under vigorous stirring. After a reaction of 15 min, a strong green colloidal $CsPbBr_3$ QDs solution was obtained. For the synthesis of $CsPbCl_{1.5}Br_{1.5}$ QDs, the method is similar to the synthesis of $CsPbBr_3$ QDs.

Fabrication of WLEDs. The dried blue-emissive $Cs_3Bi_2Br_9$/BiOBr nanocomposites were firstly mixed with the commercial yellow-emissive (Ba, $Sr)_2SiO_4:Eu^{2+}$ phosphors at a mass ratio of 1.5:1 in a polydimethylsiloxane encapsulant (Dow Corning, SYLGARD 184 Silicone Elastomer) to obtain a homogeneous mixture. Then, the mixtures were put in a vacuum chamber to get rid of the bubbles inside. Finally, the mixtures were dropped onto the window of the UV-LED chips (365 nm) and then solidified in a vacuum oven at 40 °C for 60 min and at 110 °C for 100 min sequentially, and finally the WLED was obtained. The thickness of the dried mixture films was measured by a micrometer caliper to be about 500 μm.

Characterizations. The microstructures of the as-synthesized perovskite QDs were characterized using a high-resolution TEM (JEOL, JEM-3010). The crystallinity characterizations of $Cs_3Bi_2X_9$ QDs were analyzed by XRD (Panalytical X'Pert Pro). The chemical compositions of the products were analyzed by EDS attached to TEM. The optical properties of the products were measured using a Shimadzu UV-3150 spectrophotometer and steady-state PL spectra (Horiba; Fluorolog-3) with an excitation line of 340 nm. A closed-cycle helium cryostat (Jannis; CCS-100) was used to carry out the PL measurement at different temperatures. The absolute PL quantum yield of the $Cs_3Bi_2Br_9$ QDs solution was measured by using a fluorescence spectrometer (Horiba; FluoroMax-4) with an integrated sphere (Horiba;

Quanta-φ). A pulsed NanoLED (Horiba; 340 nm) was used to conduct the transient-state PL measurement. Note that the measured absorption spectrum, PL spectrum, and time-resolved PL decay curve of the $Cs_3Bi_2X_9$ QDs at RT were performed with the colloidal solution. The emission performance of the WLEDs were carried out by using a Keithley 2400 source and a PR650 SpectraScan spectrophotometer (Photo Research) in air and at RT.

Computational methods. The first-principle calculations were carried out by using plane-wave pseudopotential approach within density functional theory as implemented in the Vienna Ab-initio Simulation Package (VASP). The electronic wave-functions are expanded in plane-wave basis sets with kinetic energy of 400 eV. The *k*-point meshes with grid spacings of $2\pi\times0.02$ $Å^{-1}$ or less is used for electronic Brillouin zone integration. The electron-ion interactions is described by means of projected augmented wave pseudopotentials with $5s^25p^66s$ for Cs, $6s^26p^3$ for Bi, $4s^24p^5$ for Br as valence electrons. The crystal structures of $CsPbBr_3$, $CsPb_2Br_5$, $Cs_3Bi_2Br_9$ were fully relaxed until the total force on each atom was less than 0.01 eV/Å. The diffusion barriers were calculated using nudged elastic band (NEB) method in conjunction with the climbing image method.

Lifetime calculation from time-resolved PL decay results

In this case, the time-resolved PL decay curves of $Cs_3Bi_2Br_9$ QDs were fitted with a biexponential function of time (t):

$$R(t) = K_1 \exp^{(-t/\tau_1)} + K_2 \exp^{(-t/\tau_2)} \quad (1)$$

where K_1 and K_2 are the distribution coefficients and, τ_1 and τ_2 stand for the characteristic PL decay lifetimes. The average lifetime ($\tau_{ave.}$) was estimated with the K_i and τ_i values from the fitted curve data according to the following equation:

$$\tau_{ave.} = \sum K_i \tau_i^2 / \sum K_i \tau_i \text{ , } i = 1, 2 \quad (2)$$

Optical images of the $Cs_3Bi_2X_9$ QDs solutions ($X = Cl_xBr_yI_{1-x-y}$, $0 \leq x, y \leq 1$)

Figure S1. Optical images of the colloidal $Cs_3Bi_2X_9$ QDs solution under ambient light with different halide compositions ($X = Cl_xBr_yI_{1-x-y}$, $0 \leq x, y \leq 1$).

Investigations on the XRD patterns of the $Cs_3Bi_2X_9$ QDs (X = Cl, Br, and I)

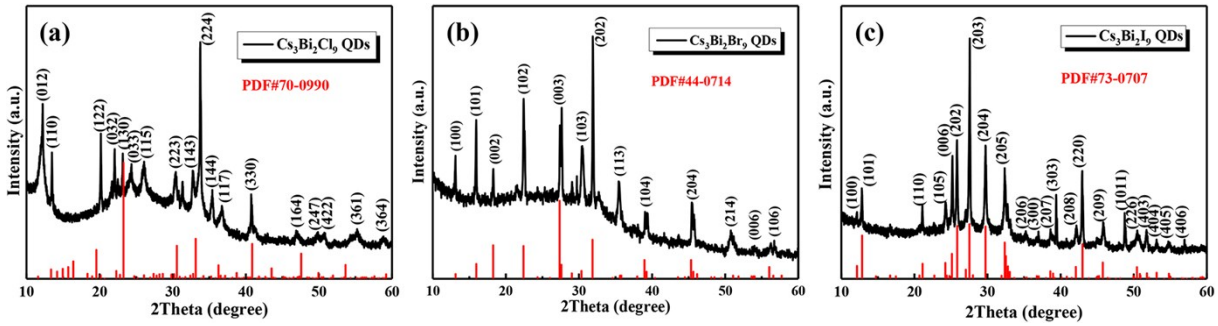

Figure S2. XRD patterns of (a) $Cs_3Bi_2Cl_9$, (b) $Cs_3Bi_2Br_9$, and $Cs_3Bi_2I_9$ QDs, respectively.

Investigation on the thermal stability of the $Cs_3Bi_2Br_9$ QDs

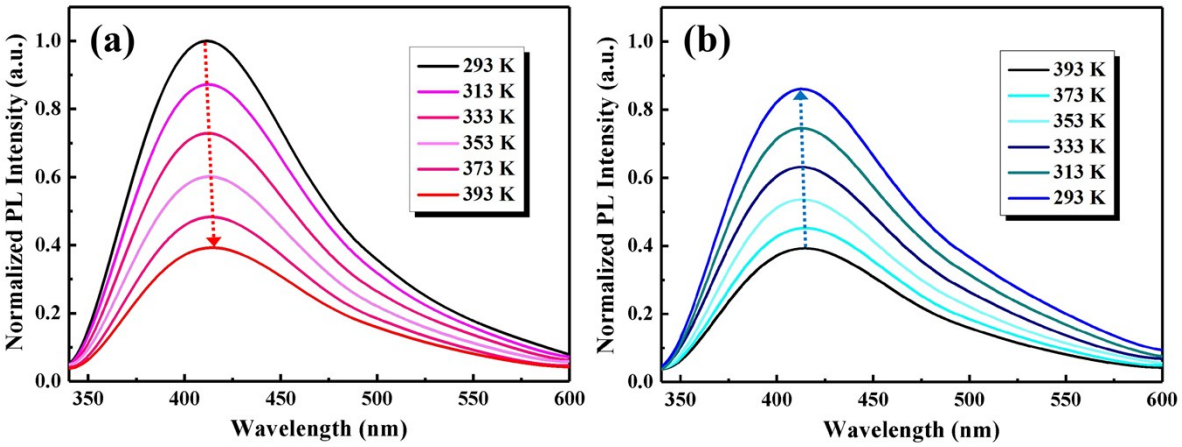

Figure S3. Normalized PL spectra of the $Cs_3Bi_2Br_9$ QDs film at different temperature over (a) the heating cycle and (b) cooling cycle.

As shown in Figure S3a, the normalized PL intensity of $Cs_3Bi_2Br_9$ QDs films decreases by ~60% with the temperature rises from 293 to 393 K. As the temperature decreases from 393 to 293 K, the PL intensity can recover to ~86% of the initial value, as shown in Figure S3b.

Comparison on the thermal stability of the $Cs_3Bi_2Br_9$ and $CsPbBr_3$ QDs

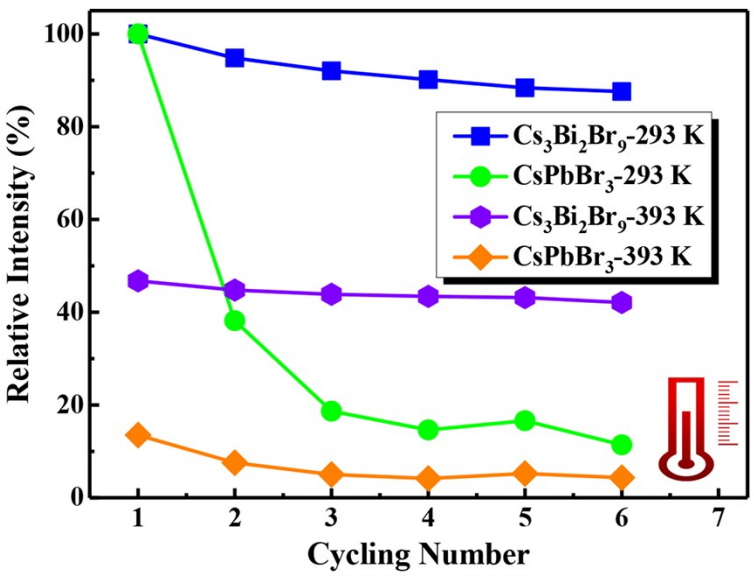

Figure S4. Integrated PL intensity of the $Cs_3Bi_2Br_9$ and $CsPbBr_3$ QDs at two representative temperature points (293 and 393 K) over six heating/cooling cycling measurements.

Comparison on the photostability of the $Cs_3Bi_2Br_9$ and $CsPbBr_3$ QDs

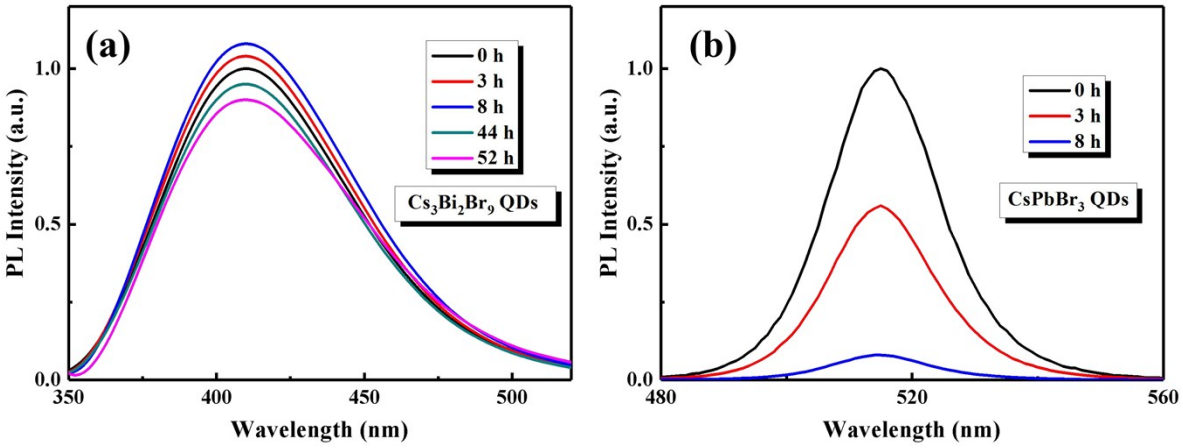

Figure S5. Normalized PL spectra of (a) the $Cs_3Bi_2Br_9$ and (b) $CsPbBr_3$ QDs solutions irradiated at different time periods under UV light (365 nm, 30 W).

As shown in Figure S5a, the PL intensity of the $Cs_3Bi_2Br_9$ QDs is slightly increased after a continuous exposure to UV light for 8 h, and then decreases to ~90% of the initial value. While, the PL intensity of $CsPbBr_3$ QDs rapidly decays under UV light irradiation, and only ~10% remains after a much shorter period of 8 h, as shown in Figure S5b.

Comparison on the moisture stability of the $Cs_3Bi_2Br_9$ and $CsPbBr_3$ QDs

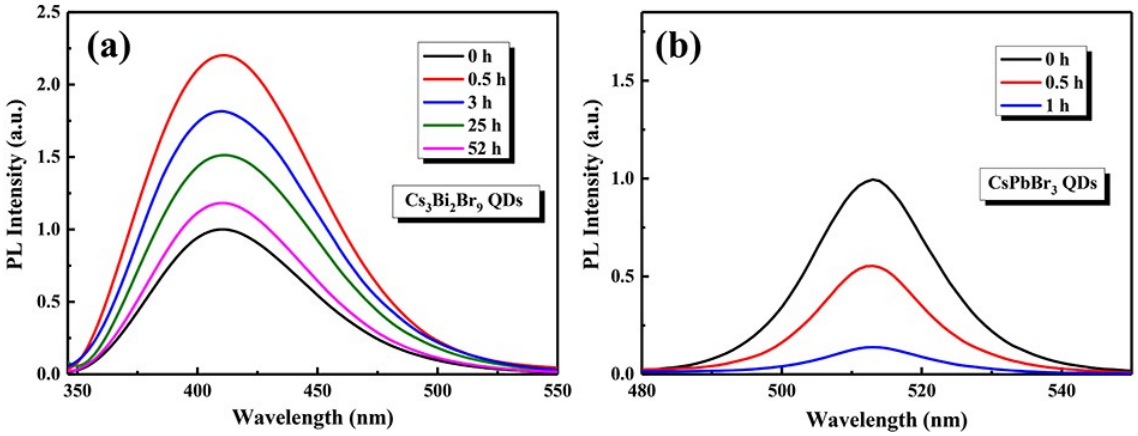

Figure S6. PL spectra of (a) the $Cs_3Bi_2Br_9$ and (b) $CsPbBr_3$ QDs solutions measured at different time periods after adding deionized water.

As shown in Figure S6a, the PL intensity of the $Cs_3Bi_2Br_9$ QDs is rapidly increased by ~130% in the initial period, and then decreases to ~115% of the initial value after 52 h continuous test. While, the PL intensity of $CsPbBr_3$ QDs drops rapidly, and only ~5% remains after 1 h test, as shown in Figure S6b.

Investigation on the moisture stability of $CsPbBr_3$ and $Cs_3Bi_2Br_9$ QDs after water treatment

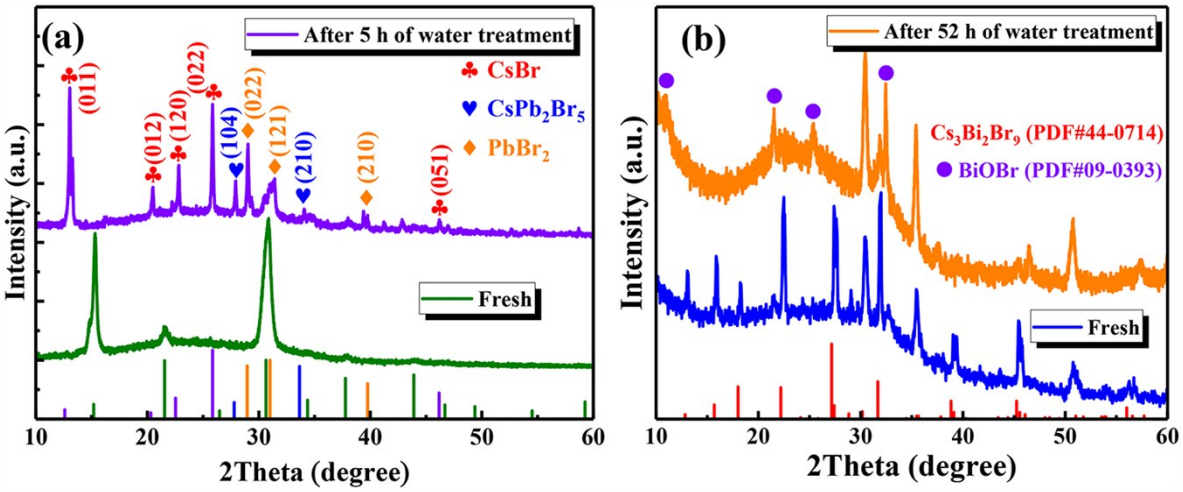

Figure S7. Evolution of the XRD patterns of (a) the $CsPbBr_3$ and (b) $Cs_3Bi_2Br_9$ QDs after water treatment.

Analysis of the chemical composition of the $Cs_3Bi_2Br_9$ QDs

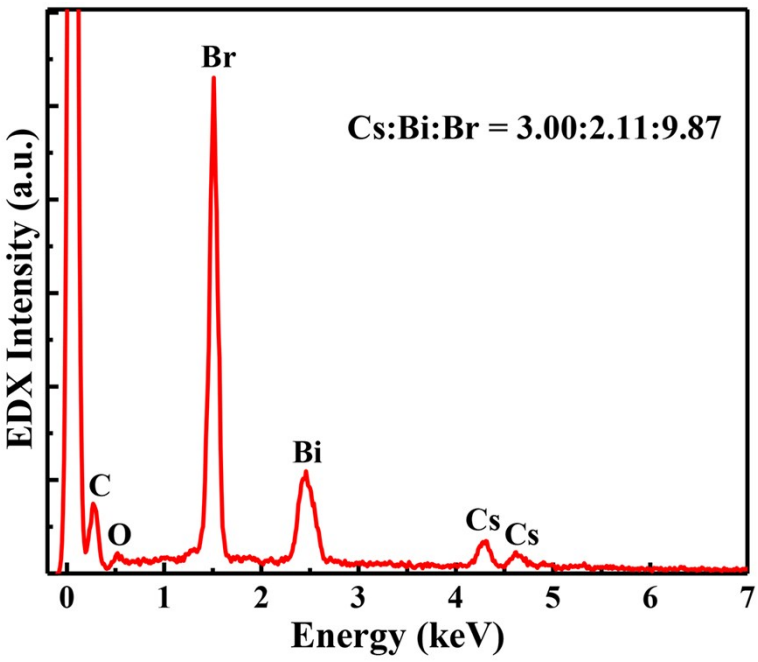

Figure S8. EDS spectra of the $Cs_3Bi_2Br_9$ QDs.

Figure S8 presents the EDS spectrum of the as-prepared $Cs_3Bi_2Br_9$ QDs. No other chemical impurities were detected in the resulting sample except for the well-known compositions, and the quantitative analysis of EDS spectrum gives the quantitative atomic ratio (%) of Cs:Bi:Br is 3.00:2.11:9.87, which is much higher than their stoichiometric ratio. Thus, the obtained $Cs_3Bi_2Br_9$ QDs showed $BiBr_x$-rich composition.

Comparison on the optical properies of the $Cs_3Bi_2X_9$ QDs before and after water treatment

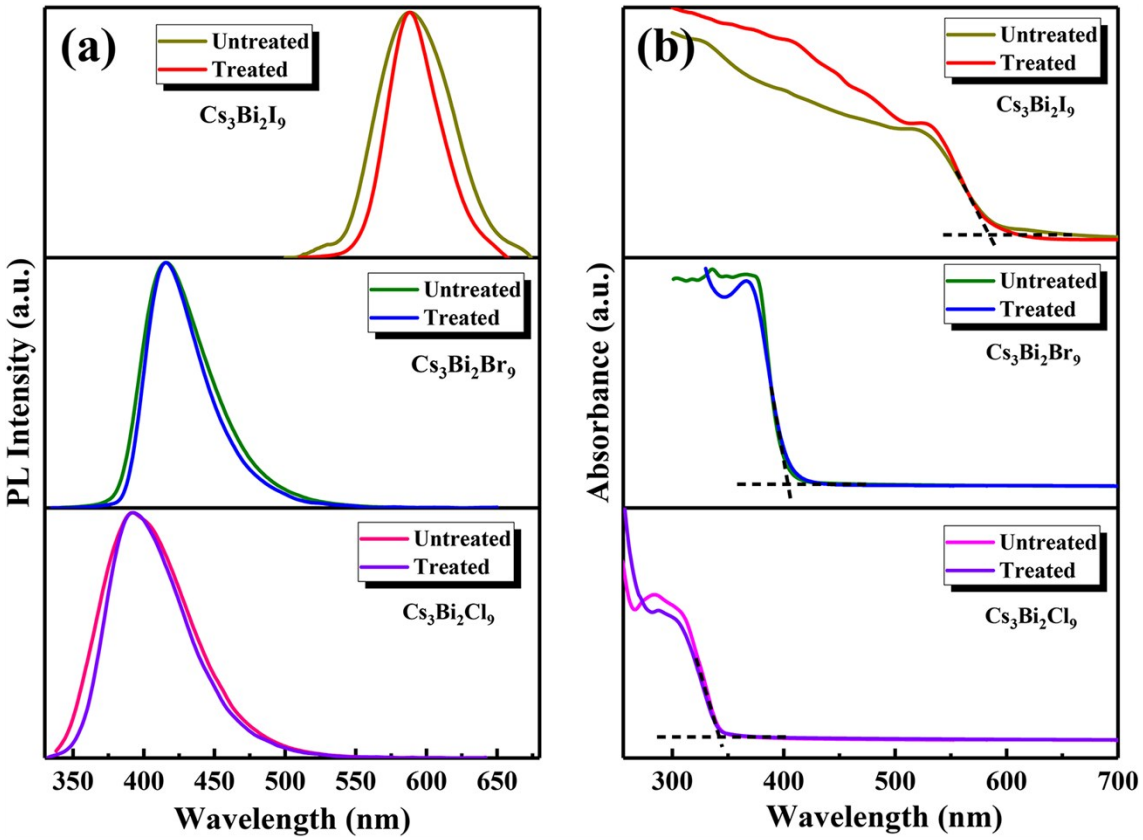

Figure S9. (a) PL and (b) absorption spectra of different $Cs_3Bi_2X_9$ QDs before and after water treatment.

PL spectra of two emission components for WLED fabrication

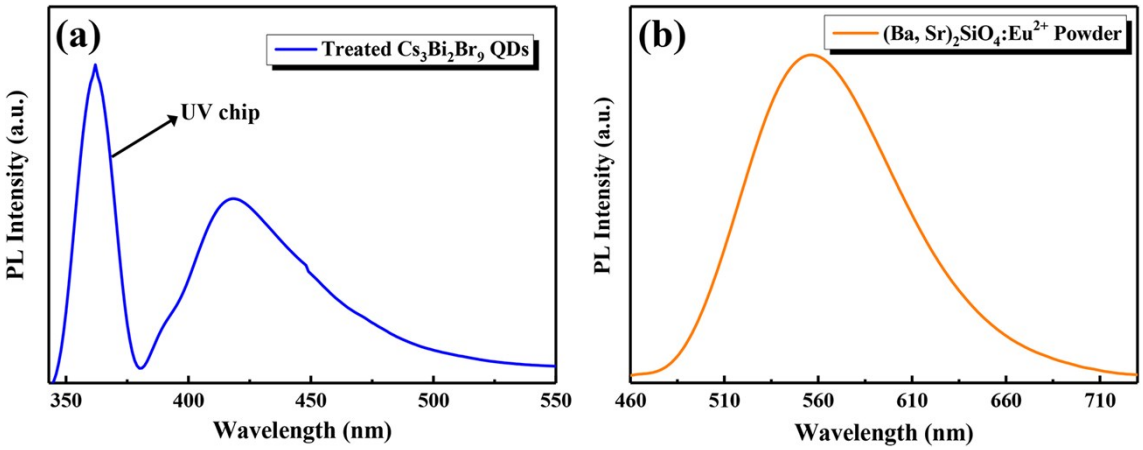

Figure S10. PL spectra of (a) the $Cs_3Bi_2Br_9$ QDs and (b) $(Ba, Sr)_2SiO_4:Eu^{2+}$ powder under UV chip (365 nm) excitation.

Shift of the CIR color coordinates of the reference WLED

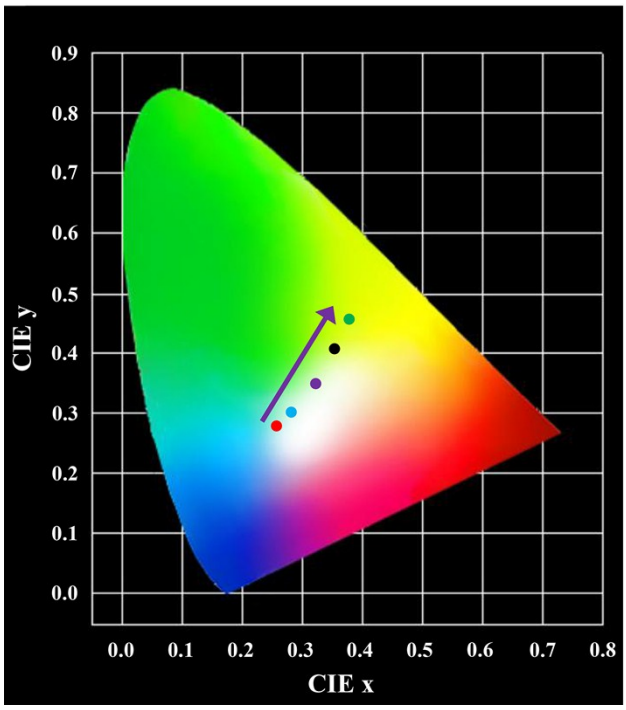

Figure S11. CIE color coordinates of the reference WLEDs at different running time.

Table S1 Detailed data of PL emission peak and FWHM of the $Cs_3Bi_2X_9$ QDs ($X = Cl_xBr_yI_{1-x-y}$, $0 \leq x, y \leq 1$)

QDs composition	Emission peak (nm)	FWHW (nm)
$Cs_3Bi_2Cl_9$	393	60
$Cs_3Bi_2Cl_{4.5}Br_{4.5}$	401	63
$Cs_3Bi_2Br_9$	411	48
$Cs_3Bi_2Br_{7.5}I_{1.5}$	425	65
$Cs_3Bi_2Br_6I_3$	442	64
$Cs_3Bi_2Br_{4.5}I_{4.5}$	472	68
$Cs_3Bi_2Br_3I_6$	493	74
$Cs_3Bi_2Br_{1.5}I_{7.5}$	540	84
$Cs_3Bi_2I_9$	590	66

Table S2 Summary of the bond length and distortion angle of $CsPbBr_3$ and $Cs_3Bi_2Br_9$

Bond length of Pb-Br	Distort angle of Br-Pb-Br	Bond length of Bi-Br	Distort angle of Br-Bi-Br
2.93 Å	180°	Bi-Br1=2.75 Å Bi-Br2=2.96 Å	174°

Table S3 Detailed CIE (x, y) and CCT (K) data of the reference WLED at different running time

working time (h)	CIE (x, y)	CCT (K)
0	0.277, 0.293	10048
0.1	0.284, 0.303	8952
0.3	0.324, 0.352	5862
0.5	0.345, 0.406	5155
0.8	0.361, 0.452	4849